의과학석사 학위논문

H9c2 세포에서 허혈-재관류 시뮬레이션 동안의 불안정 철 변화

Changes in Labile Iron Pool during Simulated Ischemia-Reperfusion of H9c2 Cells

울 산 대 학 교 대 학 원

의 과 학 과

이 동 주

Changes in Labile Iron Pool during Simulated Ischemia-Reperfusion of H9c2 Cells

지 도 교 수 김 영 훈

이 논문을 의과학석사 학위 논문으로 제출함

2021년 2월

울 산 대 학 교 대 학 원

의 과 학 과

이 동 주

이동주의 의과학석사 학위 논문을 인준함

심사위원 김 승 환 인

심사위원 이 혜 경 인

심사위원 김 영 훈 인

울 산 대 학 교 대 학 원

2021년 2월

Abstract

Recently, we developed a simulated ischemia-reperfusion (SIR) model using H9c2 cardiac myoblast cell line. Unlike traditional oxygen-glucose deprivation (OGD) models in which serum was also excluded during simulated ischemia (SI), we simulated ischemic condition by hypoxia combined with lactic acidosis and included dialyzed fetal bovine serum (diFBS). In this model, we confirmed simulated reperfusion (SR)-induced necrotic cell death, which had not been observed in former OGD models. On the other hand, it has been reported that ischemia/reperfusion (I/R)-induced injury was associated with labile iron-dependent Fenton reaction. However, whether labile iron pool (LIP) is changed during ischemia or reperfusion, is controversial. Therefore, we attempted to monitor the changes in LIP during SIR and investigate the association with SR-induced necrotic cell death using the newly developed SIR model. After SI for 24 hours, cells were incubated in a normal culture medium for 17 hours for SR. We measured lactate dehydrogenase (LDH) release to estimate the necrotic cell death during SIR. And found that LDH release was rapidly increased in the early phase of SR. Meanwhile, LIP was measured with the calcein-acetoxymethyl ester (AM) (a fluorescent iron chelator). In results, total LIP was significantly increased during SI. The increased LIP included a significant level of Fe^{3+}, which was practically undetectable in normal cells. We observed that the Fe^{2+} was further oxidized to Fe^{3+} for 1 hour of SR. The total LIP level was not changed while the Fe^{2+} was lowered and Fe^{3+} was increased. These changes implied Fenton reaction which might be associated with lipid peroxidation. To observe lipid peroxidation, we used BODIPY C11 (a lipid peroxidation probe) during SR, and found that lipid peroxidation occurred in early phase of SR. In the next step, we investigated which iron sources contribute to the increase of LIP during SI. It is well known that most intracellular iron is present as ferritin (an iron storage protein) form or heme protein form. We investigated whether bafilomycin A1 (Baf A1, a V-ATPase inhibitor) could inhibit the increase of LIP, possibly via inhibition of autophagy-mediated ferritin degradation during SI. Baf A1 partially suppressed the increase of LIP during SI and decreased SR-induced damages. We also examined whether zinc protoporphyrin (ZnPP, a heme

oxygenase-1 inhibitor) could inhibit the increase of LIP, possibly via inhibition of HO-1-mediated heme degradation during SI. ZnPP decreased elevation of LIP and decreased SR-induced damages. In summary, we developed the SIR model and investigated the changes in LIP during SIR. We found that the LIP was increased during SI, a significant portion of which was oxidized to Fe^{3+} in the early phase of SR. It was also shown that these changes in LIP were accompanied by lipid peroxidation and cell death.

Contents

List of figures

List of tables

Introduction

Reperfusion-induced cell death after myocardial ischemia, which is dependent on the duration of ischemia and residual blood flow (1-3). Oxygen-derived free radicals are produced in the early stage of reperfusion (4). However, it is unclear which mechanisms contribute to reperfusion-induced generation of lethal oxygen radicals. The traditional *in vitro* research on mechanism of ischemia/reperfusion (I/R) injury was used oxygen-glucose deprivation (OGD) model with serum-free condition (Table 1). However, the OGD model did not reflect reperfusion injuries such as reperfusion-induced reactive oxygen species (ROS) generation and accelerated lactate dehydrogenase (LDH) release (3, 5). For these reasons, we have developed *in vitro* model for simulated ischemia-reperfusion (SIR). In ischemia conditions, cells were exposed to hypoxia and produced adenosine triphosphate (ATP) and lactic acid via anaerobic metabolism (3, 6, 7). Moreover, we have reported that serum deprivation did not show simulated reperfusion (SR)-induced cell damages (8). We used dialyzed fetal bovine serum (diFBS) to control pH, glucose concentration during simulated ischemia (SI) (8). Because glucose deprivation *per se* induced severe cell death, the medium for SI was supplemented with 1 g/L of glucose. In this model, we found SR-induced necrotic cell death.

Iron is an essential micronutrient that has a wide range of redox potential (9). It makes iron an indispensable factor for numerous biological processes such as oxygen transport and storage, metabolism of proteins**,** and synthesis of genetic materials (10, 11). Because of these characteristics of iron, all aerobic organisms are exposed to the risk of ROS which is generated as a byproduct of cellular metabolism (12). Most of the iron in living cells is presented as tightly bound forms of metalloprotein such as hemoglobin or myoglobin (13), or storage forms in ferritin or non-heme iron (11). In addition, a chelatable labile iron pool (LIP) is the main source of synthesis for iron-bound proteins. Moreover, LIP is presented as non-protein bound forms, which is only a minor fraction of total iron (14, 15). In the biologic system, cells produce hydrogen peroxide and superoxide which are able to convert to a

lethal hydroxyl radical (12, 16). In this reaction system, Fe^{3+} is reduced to Fe^{2+} by superoxide, which is called the Haber-Weiss reaction (17). Reactive hydroxyl radicals can be generated from the reaction of hydrogen peroxide with Fe^{2+} (16), which is called Fenton reaction. Fenton reaction-mediated hydroxyl radicals can induce lipid peroxidation on poly unsaturated fatty acid of lipid membrane (18-20).

Fang. *et al.* have reported that ischemia/reperfusion (I/R)-induced injury is related to free iron. Another report suggested involvement of ferroptosis, which is iron-dependent cell death accompanied by lipid peroxidation by Fenton reaction (19). Iron-loaded hearts were more susceptible to damage by reperfusion, even with anoxia (21). Some studies have suggested that chelatable and catalytic iron content is increased in ischemic heart (22) or lung (23) homogenates of the rat. It was reported that LIP was increased in 2 hours after cardiac ischemia in dogs (24). For these reasons, deferoxamine (DFO, an iron chelator) was used in the clinical study of cardiac I/R injury (25). However, DFO treatment inhibited only oxidative stress by redox-active iron without reducing infarct size (25). These authors assumed that DFO might not achieve sufficient concentration in the ischemic myocardium. In addition, Baliga. *et al.* have reported that elevation of LIP shown after 1 hour of reperfusion of kidney but not during ischemia condition (26). DFO might not be sufficiently inhibit injury by reperfusion. In other words, the changes in LIP remain unclear during I/R. In these reports, tissue homogenates may not reflect the intracellular environment condition during ischemia. For these reasons, it is hard to investigate iron homeostasis using tissue homogenate samples alone. Based on these studies, we tried to monitor changes in LIP during SIR using the recently developed fluorescence iron chelator method. We investigated these changes related to SR-induced damages and which iron sources contribute to these changes.

Materials and methods

Materials

The H9c2 cell line was purchased from American Type Culture Collection (ATCC; Rockville, MD). Fetal bovine serum (FBS) and penicillin/streptomycin were purchased from Gibco (Grand Island, NY, USA). Low glucose Dulbecco's Modified Eagle's Medium (DMEM; Catalog number 30021.01) was purchased from Hyclone (Logan, UT, USA). Snakeskin dialysis tubing (Catalog number 68100), Pierce BCA protein assay kit (Catalog number 23225), calcein-acetoxymethyl ester (AM) (Catalog number C3100MP), BODIPY 591/581 C11 (Catalog number D3861) were purchased from Thermo Scientific (Waltham, MA, USA). Pyridoxal isonicotinoyl hydrazone (PIH; catalog number 737-86-0) was purchased from Sigma Aldrich (Merck Millipore, Darmstadt, Germany). Ferritin ELISA kit (Catalog number LS-F7729) was purchased from Lifespan BIoSciences (Seattle, WA, USA). DMEM (Catalog number D5030) was used during SI. Deferoxamine (DFO), ferrostatin-1 (Fer-1), necrostatin-1 (Nec-1), bafilomycin A1 (Baf A1), 2,2'-bipyridyl (BIP), and zinc protoporphyrin (ZnPP) were purchased from Sigma-Aldrich (St. Louis, MO, USA). Other materials were purchased from Sigma-Aldrich (St. Louis, MO, USA).

Cell culture and treatment

The cell line H9c2 was derived from rat embryonic cardiac myoblasts and immortalized. Cells were cultured in DMEM supplemented with 10% FBS. Cells were grown under an atmosphere of 5% CO_2 at 37 C. The culture medium was replaced with fresh DMEM every 2 days. The cultures were passed after 80% of confluences. Cells were rinsed with phosphate-buffered saline (PBS) solution and the cells exposed to trypsin and EDTA solution. The cell suspension was centrifuged at 380 x g force for 5 minutes. Pellets were re-suspended with DMEM containing 10% FBS. The cell suspension inoculated into a new 75 mm^2 culture flask for maintaining in the concentration of 3 x 10^5 cells/ml, a 35 mm dish for assessment of LDH release in SIR in the concentration of 4 x 10^5 cells/ml. The concentration of Baf

A1, DFO was described in the previous study (8). The concentration of ZnPP was described in the previous study (27, 28).

FBS dialysis

FBS dialysis protocol was followed in the previous study (8). FBS was filled into a Snake Skin dialysis tube and sealed. The tube was placed in 5 L PBS and stirred at 4 C. PBS was changed with a new PBS every 12 hours for 3 days.

SIR *in vitro* model using H9c2 cells

The *in vitro* model for SIR using H9c2 cells has been reported by Son. *et al.* (8). Every media for simulated ischemia (SI) study used DMEM supplemented with 1 g/L glucose, 4 mM L-glutamine, 10% dialyzed fetal bovine serum. For the physiological simulation of ischemic heart condition, the SI medium was supplemented with 2.4 mM $NaHCO_3$ and 21.6 mM sodium lactate. The SI medium was pre-incubated in a hypoxia chamber (MIC-101, Billups-Rothenberg Inc.) 5% CO_2, 95% N_2 balanced gas at 37 C at least 3 hours. The cells were exposed to a pre-incubated SI medium and incubated in a hypoxia chamber, an atmosphere of 5% CO_2, 95% N_2 balanced gas at 37 C for 24 hours. After SI, cells were exposed to DMEM contained with 10% fetal bovine serum for SR. Control medium was supplemented with 24 mM $NaHCO_3$ without sodium lactate and hypoxic preconditioning. In acidosis, medium was used with non-hypoxic SI medium. Hypoxia medium was used with control medium with hypoxic pre-conditioning.

Measurement of LIP

LIP assay is described in the previous study (29). Cells were washed with PBS buffer twice and treated with 250 nM calcein-AM for 5 minutes in pre-warmed 20 mM HEPES buffered Krebs solution containing 1 mg/ml BSA at 37 C, in dark. The cells were washed with pre-warmed PBS once and trypsinized. Cells were centrifuged 380 x g force and re-suspended with pre-warmed 20 mM HEPES

buffered Krebs solution containing 1 mg/ml BSA. Cells were transferred to a stirred, thermostated (37 C) cuvette. A signal is monitored at excitation 495 nm, emission 515 nm. The cells were treated with 100 μM of BIP in 50 sec and monitored 50 - 500 sec. The cells were treated with 100 μM of PIH in 500 sec and 800 sec. Fluorescence was monitored for 500 - 800 sec and 800 - 900 sec. PIH blank value was calculated with two-point values (900 sec - 800 sec). BIP value represents Fe^{2+} and ΔPIH (value of 800 - 500 sec) value represents Fe^{3+}. The total iron was summed with Fe^{2+} and Fe^{3+} values. This study used relative arbitrary unit (A.U.) that represents ΔBIP; Fe^{2+} (500 - 50 sec) / 500 sec value or ΔPIH; Fe^{3+} (800 - 500 sec) / 800 sec

Measurement of LDH release

The sample of the medium was assessed for the activity of lactate dehydrogenase (LDH) which is released into the medium each hour after SI or SR as described in the previous study (8). The medium was collected and centrifuged at 21,000 x g forces for 5 minutes. Cell lysates were collected in PBS contained with 0.2% Triton X-100 and centrifuged at 21,000 x g forces for 5 minutes. The cell lysates were diluted with PBS. The samples were added to the reaction buffer (100 mM potassium phosphate buffer, pH 7.4) contained with 0.18 mM NADH and 0.6 mM sodium pyruvate. NADH was measured by spectrophotometry at 340 nm for 100 seconds. The activity of LDH to convert 1 μmole of pyruvate to lactate in 1 minute was defined as 1 unit. The concentration change per minute was calculated to estimate LDH activity. The calculation of the unit was followed as (OD of sample – OD of cell free medium or blank) x -1 / (6.32 x 5 x 2 lysate dilution factor). The present study used 6.32 as the millimolar extinction coefficient of NADH. Blank was normalized with an average of all value of data obtained in the period of the study process. Percent of necrotic cell death was calculated with released LDH / total LDH (released LDH + lysate LDH) x 100.

Measurement of protein content

Protein content was determined by pierce's bicinchoninic acid (BCA) assay kit. Cell lysates were prepared as described above. Bovine serum albumin was used to a standard curve.

Measurement of lipid peroxidation

Fluorescence change by lipid peroxidation was monitored with BODIPY 581/591 C11 dye which was described in the previous study (30). The cells were treated with pre-incubated DMEM supplemented with 10% FBS and BODIPY 3 μM for 10 minutes in a 5% CO_2 incubator at dark. The dye was washed out with PBS twice. Cells were treated with a pre-incubated serum-free Krebs-Henseleit (KH) buffer for monitoring. The fluorescence imaging was performed on Etaluma's LS620 3 color fluorescence microscope.

Measurement of heme content

The heme assay method is described in the previous study (31). For determination of heme content, cells were cultured on a 100 mm culture dish. After SI, cells were trypsinized and centrifuged in 380 x g force for 5 minutes. The pellet was washed with PBS two times and the pellet was stored in a deep freezer. The pellet was lysed with 100 μl PBS included 0.2% Triton X-100 and centrifuged 16,000 x g force for 5 minutes. 30ul of Lysates were mixed with 270ul of pre-heated 2 M oxalic acid at 60 C. The mixed lysates were prepared duplicate. One was heated at 95 C for 1 hour to generate fluorescence of iron released PPIX. Another one was used blank. After heating, the mixture was transferred into a black 96 well plate. The fluorescence was assessed at Ex 405 / Em 600 on PerkinElmer's multi-plate reader (Victor X3). The filters were used 405/10 for excitation wavelength and 579/25 for emission wavelength. Fluorescence was calculated with heated-mixture and blank. Quantitation was used hemin standard. Fluorescence was normalized to protein content.

Statistical Analysis

Unless specified, values are expressed as mean ± SEM. Statistical comparisons were assessed by unpaired Student's t-test. $P < 0.05$ was defined as statistical significance.

Results

LDH release in the newly developed SIR model

To investigate the mechanism of cardiac I/R injury, we have developed *in vitro* model (Table 1, Figure 1A) (8). To examine SR-induced necrotic cell death, we assessed LDH release after simulated ischemia (SI) or simulated reperfusion (SR). In the simulated ischemia-reperfusion (SIR) group, SR-induced LDH release was evident, while the preceding SI for 24 hours did not include significant cell death. (Figure 1B, C). LDH release was 4.19 ± 1.07 mUnit/dish during SI. In 17 hours after SR, the LDH release was 23.95 ± 3.32 mUnit/dish. To compare cell death rate, protein content was also measured (Figure 1D). In the control group, protein content was 201.65 ± 16.02 μg protein/dish. In the SIR group, protein content was 118.71 ± 15.98 μg protein/dish. In addition, we investigated the time-course of LDH release. SR-induced LDH release was rapidly increased for 2 hours after 1 hour of SR (Figure 1E). LDH release was increased from 1.99 ± 1.00 mUnit/dish to 10.45 ± 2.18 mUnit/dish for 1 hour of SR. In 3 hours after SR, LDH release was increased to 33.12 ± 4.74 mUnit/dish. After 3 hours of SR, there was no statistical difference by further LDH release. Taken together, these data suggest that the developed *in vitro* model reflects reperfusion-induced necrotic cell death, which is rapidly increased in the early phase of SR.

SR-induced iron-dependent cell death

Fang. *et al.* suggested that I/R injury is related to iron-dependent cell death, which was recently named ferroptosis (19). The authors suggested that oxidized lipid species are byproducts of ferroptosis. It has been reported that lipid peroxidation inhibitors (e.g. tocopherol or Fer-1, a ferroptosis inhibitor) (32) suppress the membrane damage during ferroptosis (33). To investigate the association between SR-induced cell death and iron-dependent cell death, we used 100 μM DFO (deferoxamine, an iron chelator), 1 μM Fer-1 (ferrostatin-1, a ferroptosis inhibitor) and 20 μM Nec-1 (necrostatin-1, a necroptosis inhibitor) during SR. DFO and Fer-1 reduced SR-induced LDH release (Figure 2A). Percent

of LDH release was calculated with released LDH amount of total LDH amount. LDH release was decreased from 39.73 ± 4.07% to 12.77 ± 2.85%. In the Fer-1 group, LDH release was 14.14 ± 0.95%. In the Nec-1 treatment, however, LDH release was not affected. LDH release was 50.73 ± 1.95% in the Nec-1 group. These data suggest that SR-induced cell death is associated with iron-dependent mechanism. SR-induced LDH release was 39.73 ± 4.07% in the DFO-free group during SI and SR. SR-induced LDH release was lowered to 6.37 ± 0.83% by DFO treatment during SI, 12.77 ± 2.85% by DFO treatment during SR, 4.17 ± 0.98% by DFO treatment during both SI and SR. there was no statistically significant among these three groups. We suggest that SR-induced LDH release is related to intracellular chelatable iron content.

Increase of Fe^{2+} during SI and oxidation to Fe^{3+} in early phase of SR

We examined changes in LIP during SIR. For this study, we used a fluorescent iron chelator. Calcein-acetoxymethyl ester (AM) is accumulated in cells and transforms to a free form. The free form of calcein has fluorescence in Ex 495 / Em 515, which is quenched by binding of iron. To detect a dequenched signal of free calcein, we used 2,2'-bipyridyl (BIP), a Fe^{2+}-specific chelator, and pyridoxal isonicotinoyl hydrazone (PIH), a Fe^{3+}-chelator. In other words, 100 μM of BIP was treated to generate the dequenched signal of Fe^{2+}. 100 μM of PIH was treated. These indicated the Fe^{3+} level. The calculation was described in the methods.

We investigated whether LIP is increased in each condition. We assessed the LIP level under lactic acidosis or hypoxia condition for 24 hours. Lactic acidosis did not induce a significant change of LIP (Figure 3A). Whereas, hypoxia condition significantly affected the LIP. Total LIP was increased from 10.69 ± 2.25 to 27.09 ± 2.83. Fe^{3+} was increased from 0.27 ± 2.00 to 13.63 ± 3.06. However, the Fe^{2+} level was not changed under hypoxia. In the SI group, acidosis with hypoxia conditions increased the LIP level. Total LIP was increased from 10.69 ± 2.25 to 43.37 ± 3.54. Fe^{2+} was increased from 11.93 ± 1.15 to 31.22 ± 2.55, and Fe^{3+} was increased from 0.27 ± 2.00 to 11.59 ± 1.95. Together, we found that acidosis has a synergistic effect on increase of LIP under hypoxia.

We also assessed LIP during SR. For 1 hour of SR, the total LIP level was remained increased (Figure 3B). Meanwhile, Fe^{2+} was decreased to 15.85 ± 1.35 and Fe^{3+} was increased to 23.19 ± 2.09, suggesting rapid oxidation of Fe^{2+} to Fe^{3+}. For 2 hours after 1 hour of SR, the total LIP was decreased to 23.46 ± 2.15. Meanwhile, Fe^{2+} was not changed, Fe^{3+} was decreased to 6.80 ± 2.30. After 3 hours of SR, the total LIP was normalized to 9.03 ± 4.72. However, Fe^{2+} was not recovered from 3.78 ± 2.41 and Fe^{3+} was not changed. These data indicated Fenton reaction via oxidation of Fe^{2+} for 1 hour of SR.

Lipid peroxidation and necrotic cell morphology in SR

Ferroptosis is characterized by the distinctive morphology (e.g., blebbing or rupture of cell membrane) and genetic regulation (e.g., RAS mediated regulation of iron homeostasis gene expression such as transferrin receptor, ferritin) (34, 35). Braughler. *et al.* have reported that the Fe^{2+} and Fe^{3+} ratio important to the initiates the reaction of radical-mediated lipid peroxidation of polyunsaturated fatty acid (PUFAs) (36). lipid peroxidation produces lethal lipid species which cause an increase of susceptibility to oxidative damages (37). Thus, we hypothesized that changes in LIP during SR caused lipid peroxidation. To examine SR-induced lipid peroxidation, The cells were directly loaded BODIPY C11 which is an oxidation-sensitive fluorescence lipid peroxidation probe (30). The image was obtained every 30 minutes in 3 hours of SR. The time-course was based on SR-induced LDH release time-course. The BODIPY C11 signal (red) was decreased during SR and the oxidized signal (green) was increased after 1 hour of SR (Figure 4A). Also, we observed blebbing of cell membrane after 60 minutes of SR (Figure 4B). Taken together with Figures 1E, 2, 3B and 4, we concluded that change of increased LIP during SI is associated with SR-induced lipid peroxidation which causes iron-dependent necrotic cell death.

Effects of Baf A1 on LIP and SR-induced cell death

We hypothesis that inhibition of increase of LIP improves SR-induced cell death. We investigated which iron source contributed to increase of LIP. First, we examined ferritin-mediated increase of LIP. Most iron is presented as heme or non-heme iron forms (38) and most non-heme iron is ferritin (iron

storage protein) iron. Autophagy is induced by hypoxia, which is well known (39, 40). Moreover, ischemic conditions or glucose deprivation induce induction of autophagy via AMP-activated protein kinase (41). Ferritinophagy is a type of autophagy which is NCOA4 pathway-mediated ferritin degradation process, which induces ferroptosis (42). For these reasons, we used Baf A1 during SI. Baf A1 and chloroquine are frequently used to study for autophagy or ferritinophagy (42, 43). As a result, Baf A1 inhibited the increase of LIP during SI (Figure 5A). In the Baf A1 group, total LIP and Fe^{2+} were less increased than the SI group. Total LIP was decreased from 56.91 ± 2.14 to 46.44 ± 3.00. While Fe^{2+} was decreased from 50.66 ± 1.97 to 38.49 ± 4.17, Fe^{3+} was not changed. LDH release was partially decreased in 17 hours after SR in the Baf A1 group (Figure 5B). In the SI group, LDH release was 20.90 ± 3.78 mUnit/dish. In the Baf A1 group, LDH release was 14.67 ± 2.85 mUnit/dish. However, protein content and lysate LDH were not statistically remained more than the SI group (Figure 5C, 5D). In conclusion, we suggest that Baf A1 attenuates SR-induced LDH release by less increase of LIP. However, this effect not dominantly alleviated SR-induced damage.

Effects of ZnPP on LIP and SR-induced cell death

We investigated whether free heme and heme oxygenase-1 (HO-1) is associated with increase of LIP or not. It has been reported that hypoxic condition induces induction of HO-1 (31, 44). HO-1-mediated heme degradation produces CO, biliverdin, and Fe^{2+} (45). Especially in cardiac tissue, heme content is higher than other tissues (46). For these reasons, we hypothesis that heme degradation by HO-1 causes elevation of LIP during SI. We examined that ZnPP (a HO-1 inhibitor) inhibits the increase of LIP and improves SR-induced cell death. The cells were treated with ZnPP during SI. As a result, ZnPP was significantly decreased the increase of LIP during SI (Figure 6A). Total LIP was considerably decreased from 57.83 ± 3.74 to 24.36 ± 4.12. Fe^{2+} was significantly decreased from 57.40 ± 4.06 to 23.76 ± 3.79. We found ZnPP inhibited increase of LIP during SI. We found that ZnPP induced apoptotic morphologic cell death in 17 hours after SR (data not shown). We measured LDH release in ZnPP group after 3 hours of SR. LDH release was significantly decreased by ZnPP. LDH release was 12.24 ± 1.85 mUnit/dish in

the SI group. In ZnPP group, LDH release was 1.97 ± 0.30 mUnit/dish (Figure 6B). To compare cell death rate, we assessed lysate LDH content and protein content. Lysate LDH was 23.77 ± 2.28 mUnit/dish in the SI group. Lysate LDH was 33.04 ± 1.77 mUnit/dish in the ZnPP group (Figure 6C). The protein content of the ZnPP group significantly less decreased (Figure 6D). Protein content was 82.14 ± 4.29 μg protein/dish in the SI group. In the ZnPP group, protein content was 96.00 ± 5.56 μg protein/dish. Taken together, we suggest that ZnPP inhibits the increase of LIP during SI, which alleviates SR-induced cell death.

Because ZnPP inhibited increase of LIP and SR-induced necrotic cell death, we investigated HO-1-mediated heme degradation during SI. However, heme content was not decreased during SI (Figure 7). In conclusion, we suggest that ZnPP alleviates SR-induced cell damages independent of heme degradation.

Discussion

The iron homeostasis area recently has been reported. The detection assay was developed and a variety of probes were identified and commercialized. This impact becomes a breakthrough in the progression of cation study, specifically about intracellular transition metal ion. We found that the labile iron pool (LIP) was increased during SI (Figure 3). Increased Fe^{2+} was oxidized to Fe^{3+} in early phase of SR. A time-course of SR-induced lipid peroxidation was coincided with changes in LIP (Figure 4). The SR-induced LDH release was also coincided with these data (Figure 1E). Although there were no statistically significant, the absolute value of LDH release was different between DFO treatment during SI and only SR (Figure 2B). We assumed that the difference associates with cell permeability of DFO and chelatable iron concentration during SI or SR, Because DFO has low cell permeability (47). We assumed that DFO inhibited SR-induced necrotic cell death *in vitro,* while there is a possibility of which DFO could not reach sufficient enough concentration *in vivo* studies.

Baf A1 was used to confirm increase of LIP via vacuolar acidification-mediated ferritin degradation, but it is not clear whether it contributed to the increase LIP during SI. Most intracellular iron is stored in ferritin or be present as heme-bound form (15). We assumed that there are two possibilities of ferritin-mediated increase of LIP. One is ferritin released iron mediates increase of LIP. It has been reported that ferritin iron is released to the cytosol by the FMN-NADH system in hypoxia with acidosis (9). Moreover, NADH is accumulated in the cytosol in hypoxic conditions (48), which leads to FMN reduction to $FMNH_2$. After, $FMNH_2$ induces the releasing iron from ferritin mediated with NADH:oxidoreductase (49, 50). However, this theory is unclear yet. Properties of FMN:NAD(P)H oxidoreductase enzyme was not known yet (50). Furthermore, this ferritin-released iron study was performed in only ferritin solution, but not used cells or lysates. For these reasons, we also considered another possibility which is the ferritin degradation-mediated increase of LIP. As noted above, autophagy is induced by ischemia or glucose deprivation (41). Moreover, hypoxia condition induces induction of autophagy-related gene

expression (39, 40). Autophagy-mediated ferritin degradation was also known (42). For these reasons, we hypothesized that Baf A1 (a V-ATPase inhibitor) decreases ferritin degradation-mediated increase of LIP during SI. LDH release was decreased by Baf A1 (Figure 5B). However, protein content and lysate LDH content were not statistically significant (Figure 5C, D). In these results, we assumed that other effects of Baf A1. Baf A1 inhibits ATPase, which is an active proton pump for acidification of the lysosome. There is a possibility of which Baf A1 inhibited transferrin-mediated iron uptake, which via endocytosis of transferrin receptor with ATPase-mediated acidification of endosome (51). For these reasons, Figure 5 data is unclear whether the transferrin-mediated mechanism was excluded. we concluded that Baf A1 data have to investigate transferrin-mediated iron uptake mechanisms.

Although ZnPP was known as a HO-1 inhibitor, there is a possibility that ZnPP had other effects. Most of the intracellular iron consists of the heme-bound form except for non-heme iron. The heme content of cardiac tissues is much more than other tissues (38, 46). HO-1 induction is related to antioxidant function in oxidative stress conditions such as hypoxia (52, 53). HO-1-mediated heme degradation produces biliverdin, CO, Fe^{2+} and biliverdin is converted to bilirubin by biliverdin reductase (BVR) (45). It has been reported that bilirubin and biliverdin cycles have antioxidant properties via the redox cycle similar to the GSH-GSSG cycle (52). H_2O_2-induced oxidative stress was decreased by adding exogenous bilirubin and a GSH synthesis inhibitor, buthionine sulfoximine (BSO) mediated ROS level was increased by RNA interference of BVR (52). It is well known that nuclear factor erythroid 2 related factor (Nrf2) has properties of multifunctional regulation for anti-oxidant including HO-1 expression (54). In normal condition, Nrf2 is present as Keap1-Nrf2 bound form which is an inactive form. In stress conditions, however, Nrf2 is translocated from cytosol to nucleus and activates antioxidant response element (ARE)-related gene such as *hmox1*, γ-glutamylcysteine ligase (GCL) which is a rate-limiting enzyme of GSH synthesis (54). Therefore, we hypothesis that HO-1-mediated heme degradation causes increase of LIP during SI. We examined whether ZnPP inhibits increase of LIP during SI. ZnPP is used in many I/R injury or hypoxia-mediated heme degradation studies (19, 55). We found that ZnPP inhibited SR-induced damages, and LIP was also decreased by ZnPP (Figure 6). We investigated that

change of endogenous heme content mediated the HO-1 inhibition effect during SI. However, intracellular heme content was not changed during SI (Figure 7). We speculated that ZnPP may have dual effects. One is well known as the HO-1 inhibitor. Another one is the exogenous source of the protoporphyrin ring. Shetfel. *et al.* have reported that HO-1 mediated antioxidant function with bilirubin induced by an exogenous substrate such as extracellular hemin without endogenous heme degradation (45). Therefore, we suggest that ZnPP affects the decrease of LIP during SI as an exogenous substrate of porphyrin ring.

Endogenous iron sources were not contributed to increase of LIP during SI. Therefore, we assumed that extracellular iron source caused the increase of LIP during SI. Transferrin is the main route of exogenous iron uptake and transferrin receptor expression also induced by hypoxia condition (56, 57). In the culture system, most of the extracellular iron content is present as serum iron which is predominantly transferrin-bound iron. Moreover, Gao. *et al.* have reported that transferrin is required to necrotic cell death by serum loaded iron (58). Although we performed a transferrin-association experiment yet, we found that endogenous iron sources did not affect predominantly the increase in LIP during SI (Figure 5-7). Therefore, we assumed that transferrin receptor-mediated iron uptake increased LIP during SI.

Regulation of iron homeostasis is an essential mechanism for cell viability. The handling of Iron is inevitable to live using aerobic metabolism. Unregulated iron will become a double-edged sword that can lead to generation of ROS via Fenton reaction with intracellular products of aerobic metabolism. For these reasons, iron metabolism is tightly regulated by the iron-responsive elements – iron regulatory protein system. In I/R injury, it is necessary for effective therapy to understand in detail what factors change and cause cell damage. We developed the optimal *in vitro* model for the study of I/R injury and we found that increase of LIP during SI causes lipid peroxidation mediated SR-induced damage in the early phase of SR.

Exp. condition	OGD model	SI model
Medium	No FBS, DMEM	10% diFBS, DMEM
A medium pH	7.4	6.4
Supplement	None	Sodium lactate
O_2	None	None
Glucose	None	1 g/L

Table 1. Comparison of experimental conditions of SI model

It is well known that ischemia causes nutrient deprivation, hypoxia and lactic acidosis (7). Serum deprivation and glucose deprivation were used to simulate nutrient deprivation in OGD model. Unlike the OGD model, diFBS was used to control the pH and glucose concentration of the medium while preventing the deprivation of growth factors and hormones caused by serum deprivation. The SI medium was supplemented with lactate and adjusted pH with $NaHCO_3$ to reflect lactic acidosis. Lactic acidosis is a critical factor to simulate reperfusion injury, which had been reported (8). The normal concentration of glucose was used to prevent severe cell damage during SI before SR. (OGD, oxygen glucose deprivation. SI, simulated ischemia. diFBS, dialyzed fetal bovine serum)

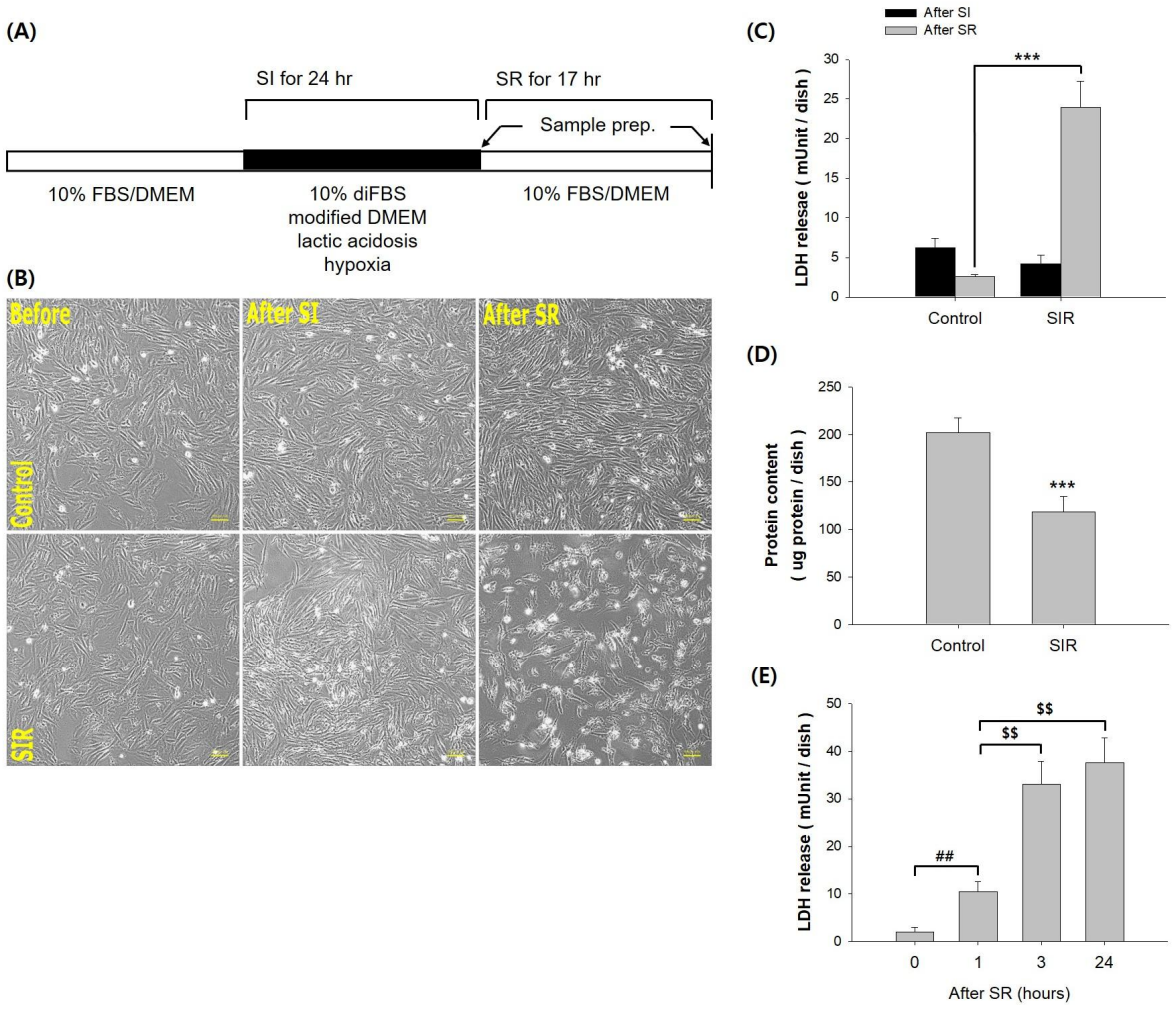

Figure 1. LDH release in the newly developed SIR model

(A) To simulate ischemia-reperfusion, the confluent H9c2 cells were exposed to SI medium for 24 hours. The SI medium was described in Table 1. Subsequently, the cells were exposed to SR medium for 17 hours. The medium for SR was used DMEM contained with 10% fetal bovine serum which is the normal culture medium (B) Cell images were obtained just before each step using a magnification microscope. Unlike the SIR group, control group used DMEM supplemented with 10% diFBS without adjusting pH with lactate and hypoxia instead of SI medium for 24 hours. Images represent morphology during SIR. (C) LDH samples were obtained from the medium after 24 hours of SI or 17 hours of SR. (n=11 to 13) (D) Cell lysate was obtained after 17 hours of SR. Protein content was determined by BCA assay. (n=11 to 13). (E) LDH samples were collected from the medium after 0, 1, 3 and 24 hours of SR

(n=6). Data were presented as mean ± SEM. $^{***}P<0.001$ was compared with control. $^{\#\#}P<0.01$ was compared with 0 hour of SR. $^{\$\$}P<0.01$ was compared with 1 hour of SR. Scale bar, 100 μm. (SIR, simulated ischemia-reperfusion. SI, simulated ischemia. SR, simulated reperfusion)

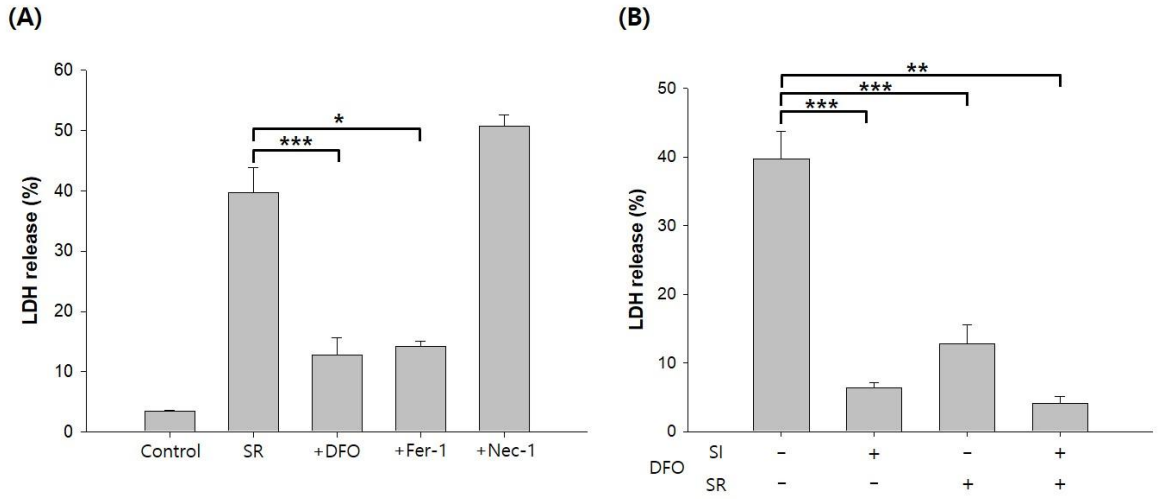

Figure 2. SR-induced iron-dependent cell death

(A) The H9c2 cells were treated with 100 μM DFO (an iron chelator), 1 μM Fer-1 (a ferroptosis inhibitor), 20 μM Nec-1 (a necroptosis inhibitor) for 17 hours of SR. LDH samples were obtained from medium after SR. Percent of LDH release was calculated with released LDH amount of total LDH amount. (n=3 to 13). (B) Cells were treated with 100 μM DFO during SI or/and SR. LDH samples were collected from medium after SI or SR (n=6 to 13). Data were presented as mean ± SEM. $^{*}P<0.05$, $^{**}P<0.01$, $^{***}P<0.001$ were compared with SIR. (SI, simulated ischemia. SR, simulated reperfusion. SIR, simulated ischemia-reperfusion. DFO, deferoxamine. Fer-1, ferrostatin-1. Ner-1, necrostatin-1)

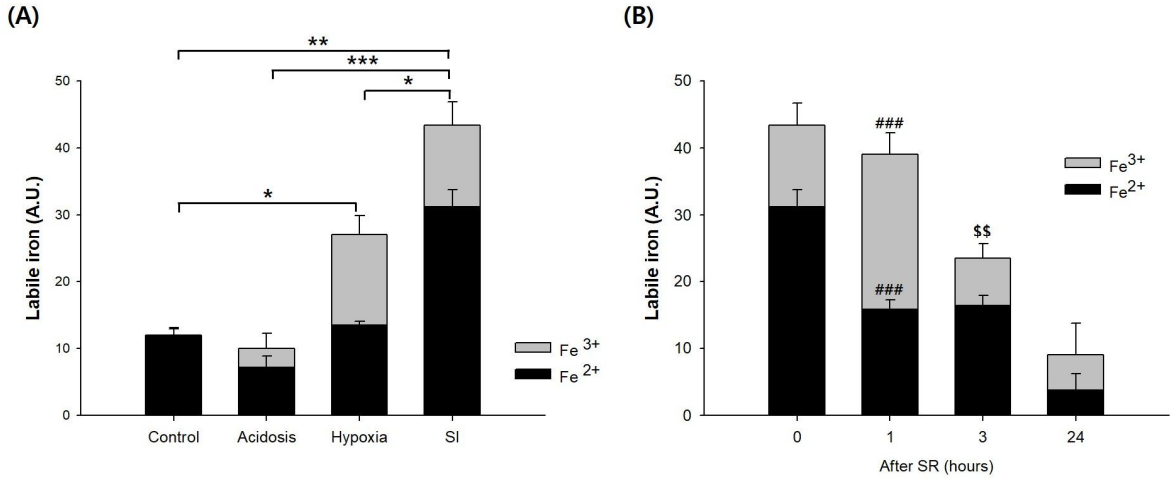

Figure 3. Increase of Fe^{2+} during SI and oxidation to Fe^{3+} in early phase of SR

To monitor LIP, calcein-AM (a fluorescence iron chelator) was loaded into the H9c2 cells after each time-course or conditions. The cells were trypsinized and transferred to a thermo-stated cuvette and stirred. The fluorescence of basal free-calcein signal was monitored at Ex 495 / Em 515 using a fluorescence spectrophotometer. Dequenched free-calcein signal was generated by BIP (a Fe^{2+}-specific chelator) and PIH (a Fe^{3+}-specific chelator) after detection of the basal signal. The calculation was described in methods. Black bars represent Fe^{2+} and grey bars represent Fe^{3+}. Total LIP was summed with the value of Fe^{2+} and Fe^{3+}. The statistical significance of the total LIP was described in the graph. (A) Control, acidosis and hypoxia were performed parallel with SI. Control group used DMEM supplemented 10% diFBS without adjusting of pH with lactate and hypoxia. Acidosis group used DMEM supplemented with 10% diFBS adjusting pH with lactate and $NaHCO_3$ without hypoxia. Hypoxia groups used DMEM supplemented with 10% diFBS without adjusting pH of medium. LIP was measured after each condition. (n=5 to 8) (B) LIP was measured each time-course during SR. Black bars represent Fe^{2+} and grey bars represent Fe^{3+}. Data were presented as mean ± SEM. $^{*}P<0.05$, $^{**}P<0.01$ and $^{***}P<0.001$ were compared with value of total iron. $^{###}P<0.001$ was compared with SR 0 hour. $^{\$\$}P<0.01$ were compared with SR 1 hour. (n=5 to 8) (SI, simulated ischemia. SR, simulated reperfusion. diFBS, dialyzed fetal bovine serum. BIP, 2,2'-bipyridyl. PIH, pyridoxal isonicotinoyl hydrazine)

(A)

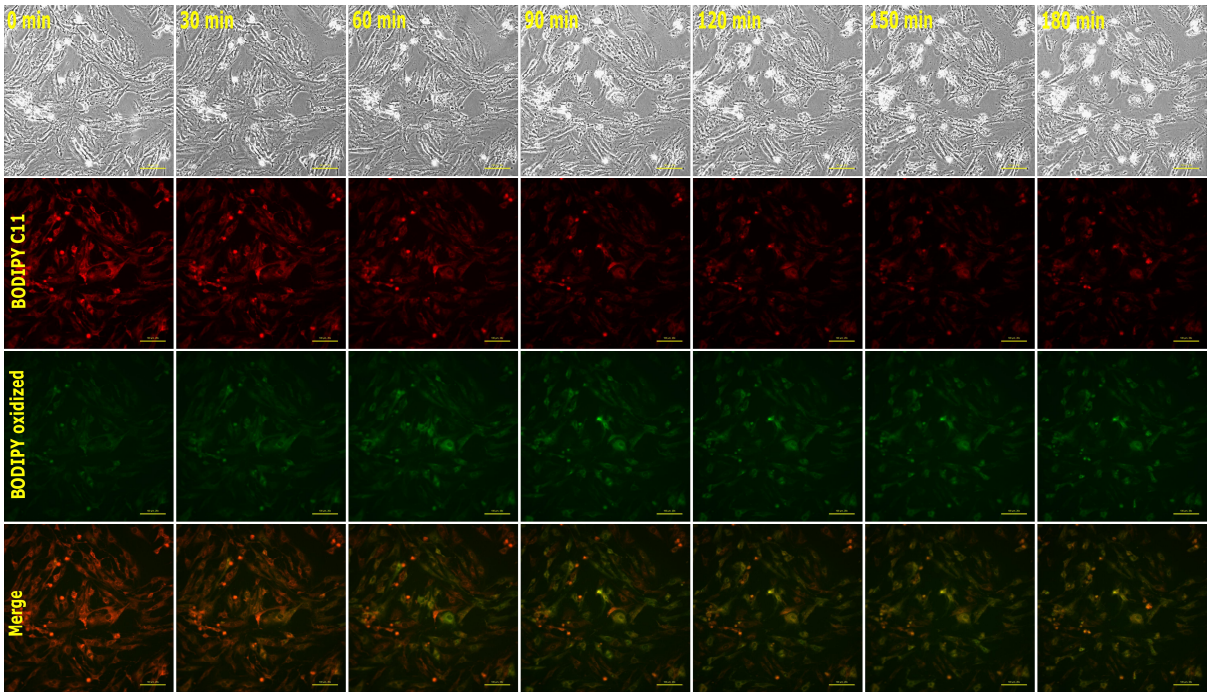

(B)

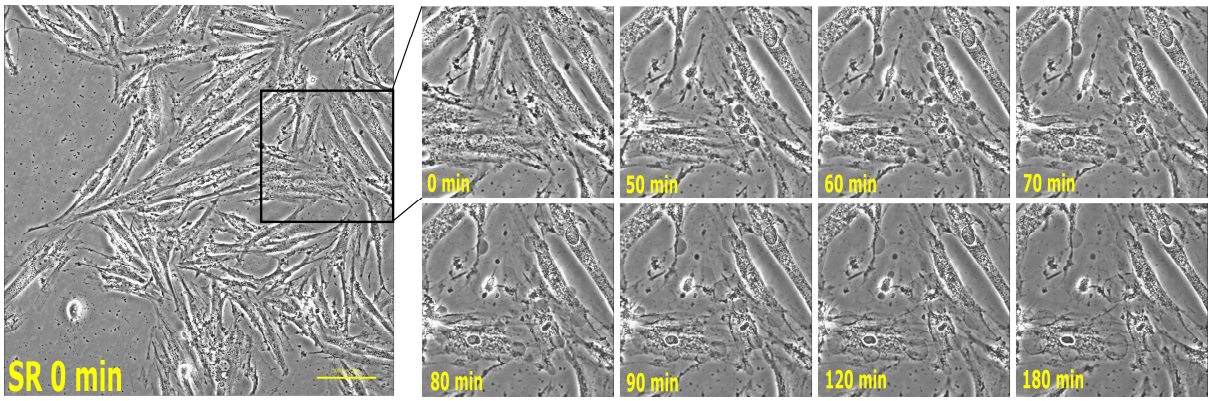

Figure 4. Lipid peroxidation and necrotic cell morphology in SR

(A) To examine SR-induced lipid peroxidation, cells were loaded with 3 μM BODIPY C11 in serum-free DMEM after SI. The cells were washed out with PBS. The cells were exposed to $NaHCO_3$ buffered KH physiologic solution to monitor lipid peroxidation. Live-cell fluorescence image was obtained every 30 minutes for 3 hours of SR. Reduced BODIPY (Red) image was obtained at Ex 581 /Em 595, BODIPY oxidized form (Green) image was obtained at Ex 485 / Em 520. (B) To observation of SR-

induced necrotic morphology, the H9c2 cell images were taken every 10 minutes of fixed field. Representative images are shown blebbing of cell membrane between 60 minutes and 90 minutes of SR. All images were obtained using Etaluma's LS620 3 color fluorescence microscope. Scale bar, 100 μm. (SR, simulated reperfusion. KH, krebs-henseleit)

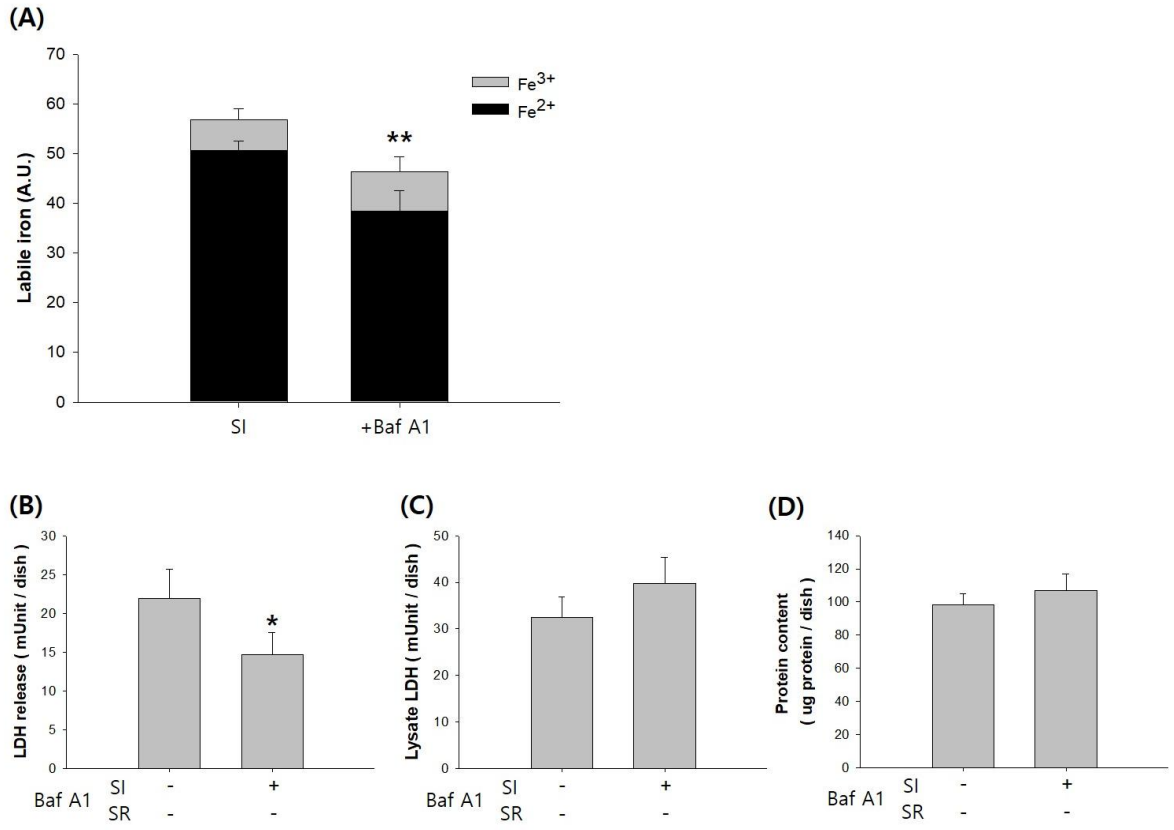

Figure 5. Effects of Baf A1 on LIP and SR-induced cell death

To investigate the association with increase of LIP and autophagy-mediated ferritin degradation via vacuolar acidification by ATPase, the H9c2 cells were treated with 1 nM Baf A1 (a V-ATPase inhibitor) during only SI. (A) LIP was measured by the calcein-AM method. The calculation of the fluorescence signal was described in methods. Black bars represent Fe^{2+}, grey bars represent Fe^{3+}. The statistical significance of the total LIP was described in the graph (n=4). (B) The H9c2 cells were treated with 1 nM Baf A1 during only SI. Thereafter, the cells were exposed to SR medium. LDH sample was obtained from each medium after 17 hours of SR. (n=8 to 10). (C) Cell lysate samples were collected after 17 hours of SR (n=8 to 10). (D) Protein content was determined by BCA assay using lysate samples. (n=8 to 10). Data are presented as mean ± SEM. $^{*}P<0.05$, $^{**}P<0.01$ were compared with the SI group. (SI, simulated ischemia. SR, simulated reperfusion. Baf A1, Bafilomycin A1)

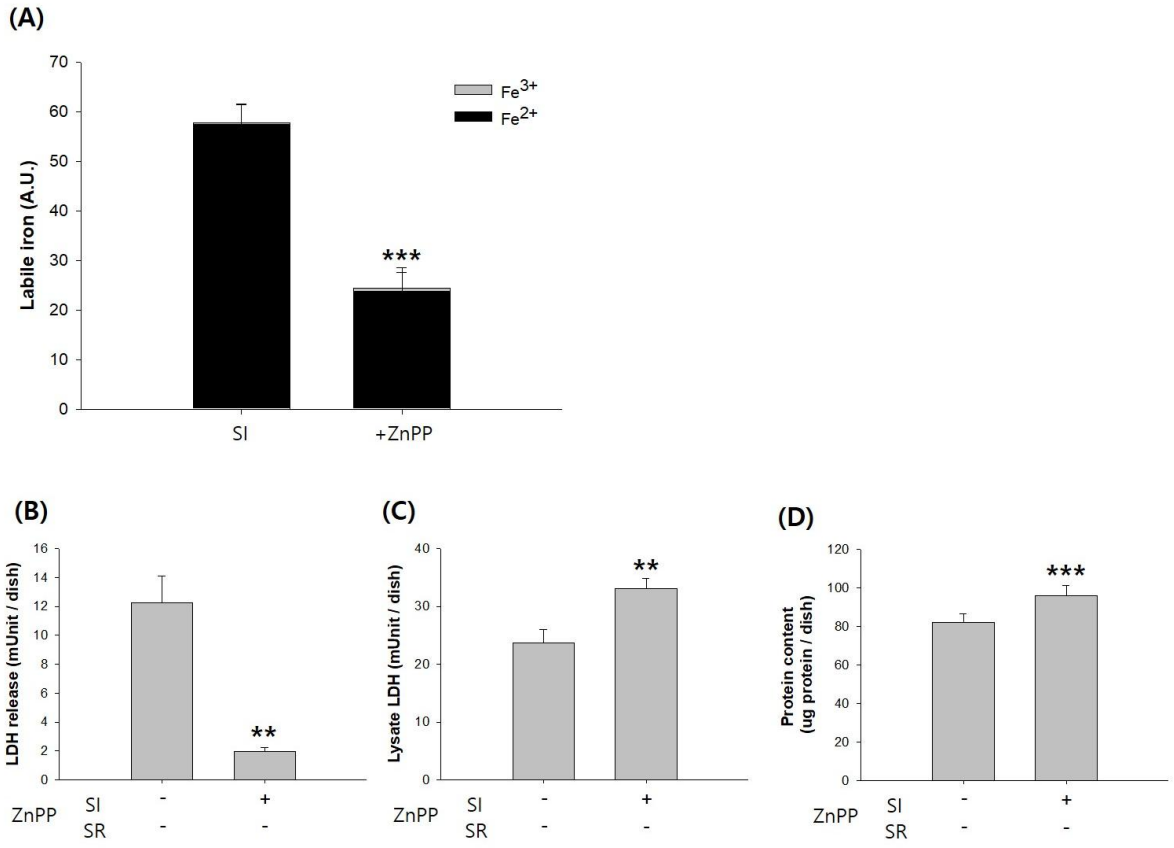

Figure 6. Effects of ZnPP on LIP and SR-induced cell death

To examine heme degradation-mediated increase of LIP, ZnPP (a heme oxygenase-1 inhibitor) group was treated with 5 μM ZnPP during only SI. (A) LIP was measured by Calcein-AM method. Black bars represent Fe^{2+} and grey bars represent Fe^{3+}. The statistical significance of the total LIP was described in the graph (n=5). (B) The H9c2 cells were treated with 5 μM ZnPP during only SI. Thereafter, the cells exposed to SR medium during SR. LDH samples were collected from each medium after 3 hours of SR (n=7). (C) Cell lysates were collected after 3 hours of SR (n=7). (D) Protein content was measured by BCA assay using cell lysates (n=7). Data were presented as mean ± SEM. $^{**}P<0.01$, $^{***}P<0.001$ were compared with SI group. (SI, simulated ischemia. SR, simulated reperfusion. ZnPP, zinc protoporphyrin)

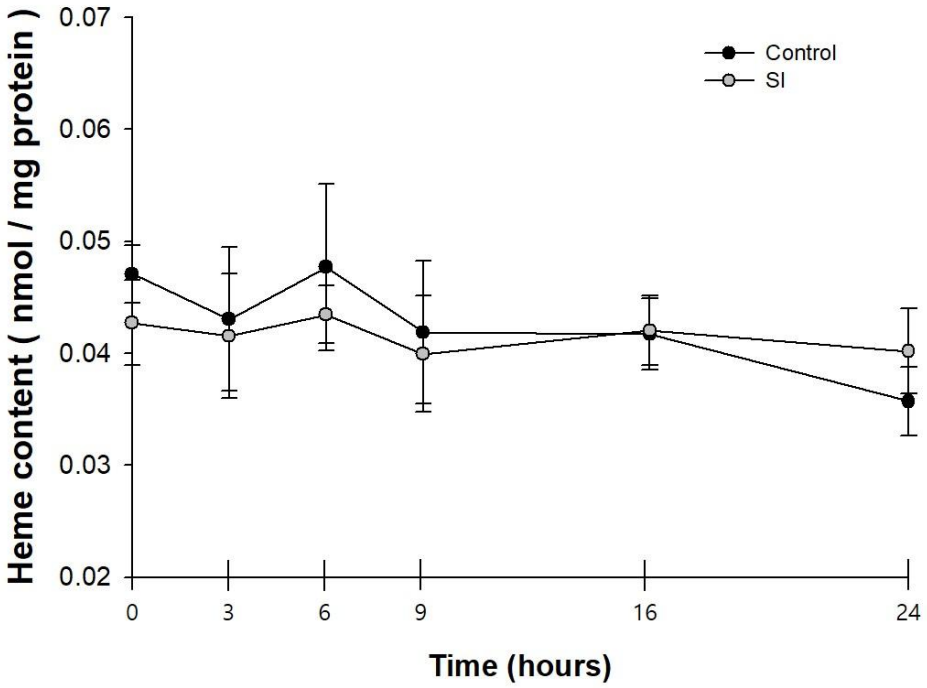

Figure 7. Changes of intracellular heme content during SI

Heme content was determined using cell lysate. The control group (black) was performed parallel with the SI group (grey). Control group used DMEM supplemented with 10% diFBS without adjusting pH and hypoxia instead of SI medium for the described time-course. The cell lysates were collected after each time of SR. The method as described above. Heme contents were normalized to protein contents. The protein contents were determined by BCA assay (n=3 to 9). Data were presented as mean ± SEM. (SI, simulated ischemia)

References

1. Yellon DM, Hausenloy DJ. Myocardial reperfusion injury. N Engl J Med. 2007;357(11):1121-1135.
2. Heusch G. Myocardial ischaemia–reperfusion injury and cardioprotection in perspective. Nature Reviews Cardiology. 2020;7:773-789
3. Hausenloy DJ, Yellon DM. Myocardial ischemia-reperfusion injury: a neglected therapeutic target. J Clin Invest. 2013;123(1):92-100.
4. Zweier JL, Flaherty JT, Weisfeldt ML. Direct measurement of free radical generation following reperfusion of ischemic myocardium. Proc Natl Acad Sci U S A. 1987;84(5):1404-1407.
5. Yang GZ, Xue FS, Liu YY, Li HX, Liu Q, Liao X. Feasibility Analysis of Oxygen-Glucose Deprivation-Nutrition Resumption on H9c2 Cells In vitro Models of Myocardial Ischemia-Reperfusion Injury. Chin Med J (Engl). 2018;131(19):2277-2286.
6. Graf H, Leach W, Arieff A. Evidence for a detrimental effect of bicarbonate therapy in hypoxic lactic acidosis. Science. 1985;227(4688):754-756.
7. Carden DL, Martin GB, Nowak RM, Foreback CC, Tomlanovich MC. Lactic acidosis as a predictor of downtime during cardiopulmonary arrest in dogs. Am J Emerg Med. 1985;3(2):120-124.
8. Son E, Lee D, Woo CW, Kim YH. The optimal model of reperfusion injury in vitro using H9c2 transformed cardiac myoblasts. Korean J Physiol Pharmacol. 2020;24(2):173-183.
9. Bou-Abdallah F, Paliakkara JJ, Melman G, Melman A. Reductive Mobilization of Iron from Intact Ferritin: Mechanisms and Physiological Implication. Pharmaceuticals (Basel). 2018;11(4):120-133.
10. Britton RS, Leicester KL, Bacon BR. Iron Toxicity and Chelation Therapy. International Journal of Hematology. 2002;76(3):219-228.
11. Paterek A, Mackiewicz U, Maczewski M. Iron and the heart: A paradigm shift from systemic to cardiomyocyte abnormalities. J Cell Physiol. 2019;234(12):21613-21629.

12. Halliwell B, Gutteridge JM. Role of free radicals and catalytic metal ions in human disease: an overview. Methods Enzymol. 1990;186:1-85.
13. Dev S, Babitt JL. Overview of iron metabolism in health and disease. Hemodial Int. 2017;21 Suppl 1:S6-S20.
14. Fontecave M, Pierre JL. Iron metabolism: the low-molecular-mass iron pool. Biol Met. 1991;4(3):133-135.
15. Mulligan M, Althaus B, Linder MC. Non-ferritin, non-heme iron pools in rat tissues. Int J Biochem. 1986;18(9):791-798.
16. Winterbourn CC. Toxicity of iron and hydrogen peroxide: the Fenton reaction. Toxicol Lett. 1995;82-83:969-974.
17. Aust SD, Morehouse LA, Thomas CE. Role of metals in oxygen radical reactions. J Free Radic Biol Med. 1985;1(1):3-25.
18. Komara JS, Nayini NR, Bialick HA, Indrieri RJ, Evans AT, Garritano AM, et al. Brain iron delocalization and lipid peroxidation following cardiac arrest. Ann Emerg Med. 1986;15(4):384-389.
19. Fang X, Wang H, Han D, Xie E, Yang X, Wei J, et al. Ferroptosis as a target for protection against cardiomyopathy. Proc Natl Acad Sci U S A. 2019;116(7):2672-2680.
20. Dixon SJ, Stockwell BR. The Hallmarks of Ferroptosis. Annual Review of Cancer Biology. 2019;3(1):35-54.
21. van der Kraaij AM, Mostert LJ, van Eijk HG, Koster JF. Iron-load increases the susceptibility of rat hearts to oxygen reperfusion damage. Protection by the antioxidant (+)-cyanidanol-3 and deferoxamine. Circulation. 1988;78(2):442-429.
22. Voogd A, Sluiter W, van Eijk HG, Koster JF. Low molecular weight iron and the oxygen paradox in isolated rat hearts. J Clin Invest. 1992;90(5):2050-2055.
23. Zhao G, Ayene IS, Fisher AB. Role of iron in ischemia-reperfusion oxidative injury of rat lungs. Am J Respir Cell Mol Biol. 1997;16(3):293-299.

24. Holt S, Gunderson M, Joyce K, Nayini NR, Eyster GF, Garitano AM, et al. Myocardial tissue iron delocalization and evidence for lipid peroxidation after two hours of ischemia. Ann Emerg Med. 1986;15(10):1155-1159.

25. Chan W, Taylor AJ, Ellims AH, Lefkovits L, Wong C, Kingwell BA, et al. Effect of iron chelation on myocardial infarct size and oxidative stress in ST-elevation-myocardial infarction. Circ Cardiovasc Interv. 2012;5(2):270-278.

26. Baliga R, Ueda N, Shah SV. Increase in bleomycin-detectable iron in ischaemia/reperfusion injury to rat kidneys. The Biochemical journal. 1993;291 (Pt 3):901-905.

27. Appleton SD, Chretien ML, McLaughlin BE, Vreman HJ, Stevenson DK, Brien JF, et al. Selective Inhibition of Heme Oxygenase, without Inhibition of Nitric Oxide Synthase or Soluble Guanylyl Cyclase, by Metalloporphyrins at Low Concentrations. Drug Metabolism and Disposition. 1999;27(10):1214-1219.

28. Chen D, Jin Z, Zhang J, Jiang L, Chen K, He X, et al. HO-1 Protects against Hypoxia/Reoxygenation-Induced Mitochondrial Dysfunction in H9c2 Cardiomyocytes. PLOS ONE. 2016;11(5):e0153587.

29. Cabantchik ZI, Glickstein H, Milgram P, Breuer W. A fluorescence assay for assessing chelation of intracellular iron in a membrane model system and in mammalian cells. Anal Biochem. 1996;233(2):221-227.

30. Drummen GP, van Liebergen LC, Op den Kamp JA, Post JA. C11-BODIPY(581/591), an oxidation-sensitive fluorescent lipid peroxidation probe: (micro)spectroscopic characterization and validation of methodology. Free Radic Biol Med. 2002;33(4):473-490.

31. Khechaduri A, Bayeva M, Chang HC, Ardehali H. Heme levels are increased in human failing hearts.J Am Coll Cardiol. 2013;61(18):1884-1893.

32. Miotto G, Rossetto M, Di Paolo ML, Orian L, Venerando R, Roveri A, et al. Insight into the mechanism of ferroptosis inhibition by ferrostatin-1. Redox Biology. 2020;28:101328.

33. Latunde-Dada GO. Ferroptosis: Role of lipid peroxidation, iron and ferritinophagy. Biochimica et

Biophysica Acta (BBA) - General Subjects. 2017;1861(8):1893-1900.

34. Dixon Scott J, Lemberg Kathryn M, Lamprecht Michael R, Skouta R, Zaitsev Eleina M, Gleason Caroline E, et al. Ferroptosis: An Iron-Dependent Form of Nonapoptotic Cell Death. Cell. 2012;149(5):1060-1072.
35. Yang WS, Stockwell BR. Synthetic Lethal Screening Identifies Compounds Activating Iron-Dependent, Nonapoptotic Cell Death in Oncogenic-RAS-Harboring Cancer Cells. Chemistry & Biology. 2008;15(3):234-245.
36. Braughler JM, Duncan LA, Chase RL. The involvement of iron in lipid peroxidation. Importance of ferric to ferrous ratios in initiation. J Biol Chem. 1986;261(22):10282-10289.
37. Feng H, Stockwell BR. Unsolved mysteries: How does lipid peroxidation cause ferroptosis? PLoS Biol. 2018;16(5):e2006203.
38. Lakhal-Littleton S. Mechanisms of cardiac iron homeostasis and their importance to heart function. Free Radical Biology and Medicine. 2019;133:234-237.
39. Luo G, Jian Z, Zhu Y, Zhu Y, Chen B, Ma R, et al. Sirt1 promotes autophagy and inhibits apoptosis to protect cardiomyocytes from hypoxic stress. Int J Mol Med. 2019;43(5):2033-2043.
40. Dai S, Xu Q, Liu S, Yu B, Liu J, Tang J. Role of autophagy and its signaling pathways in ischemia/reperfusion injury. Am J Transl Res. 2017;9(10):4470-4480.
41. Matsui Y, Takagi H, Qu X, Abdellatif M, Sakoda H, Asano T, et al. Distinct Roles of Autophagy in the Heart During Ischemia and Reperfusion. Circulation Research. 2007;100(6):914-922.
42. Hou W, Xie Y, Song X, Sun X, Lotze MT, Zeh HJ, et al. Autophagy promotes ferroptosis by degradation of ferritin. Autophagy. 2016;12(8):1425-1428.
43. Gao M, Monian P, Pan Q, Zhang W, Xiang J, Jiang X. Ferroptosis is an autophagic cell death process. Cell Res. 2016;26(9):1021-1032.
44. Lee PJ, Jiang BH, Chin BY, Iyer NV, Alam J, Semenza GL, et al. Hypoxia-inducible factor-1 mediates transcriptional activation of the heme oxygenase-1 gene in response to hypoxia. J Biol Chem. 1997;272(9):5375-5381.

45. Sheftel AD, Kim SF, Ponka P. Non-heme induction of heme oxygenase-1 does not alter cellular iron metabolism. J Biol Chem. 2007;282(14):10480-10486.
46. Rebouche CJ, Wilcox CL, Widness JA. Microanalysis of non-heme iron in animal tissues. Journal of Biochemical and Biophysical Methods. 2004;58(3):239-251.
47. Glickstein H, El RB, Shvartsman M, Cabantchik ZI. Intracellular labile iron pools as direct targets of iron chelators: a fluorescence study of chelator action in living cells. Blood. 2005;106(9):3242-3250.
48. Khan S, O'Brien PJ. Modulating hypoxia-induced hepatocyte injury by affecting intracellular redox state. Biochim Biophys Acta. 1995;1269(2):153-161.
49. Topham R, Goger M, Pearce K, Schultz P. The mobilization of ferritin iron by liver cytosol. A comparison of xanthine and NADH as reducing substrates. The Biochemical journal. 1989;261(1):137-143.
50. Melman G, Bou-Abdallah F, Vane E, Maura P, Arosio P, Melman A. Iron release from ferritin by flavin nucleotides. Biochim Biophys Acta. 2013;1830(10):4669-4674.
51. Ponka P, Lok CN. The transferrin receptor: role in health and disease. The International Journal of Biochemistry & Cell Biology. 1999;31(10):1111-1137.
52. Barañano DE, Rao M, Ferris CD, Snyder SH. Biliverdin reductase: A major physiologic cytoprotectant. Proceedings of the National Academy of Sciences. 2002;99(25):16093-16098.
53. Suttner DM, Sridhar K, Lee CS, Tomura T, Hansen TN, Dennery PA. Protective effects of transient HO-1 overexpression on susceptibility to oxygen toxicity in lung cells. Am J Physiol. 1999;276(3):L443-451.
54. Loboda A, Damulewicz M, Pyza E, Jozkowicz A, Dulak J. Role of Nrf2/HO-1 system in development oxidative stress response and diseases: an evolutionarily conserved mechanism. Cell Mol Life Sci. 2016;73(17):3221-3247.
55. Kwon M-Y, Park E, Lee S-J, Chung SW. Heme oxygenase-1 accelerates erastin-induced ferroptotic cell death. Oncotarget. 2015;6(27):24393-24403.

56. Tacchini L, Bianchi L, Bernelli-Zazzera A, Cairo G. Transferrin receptor induction by hypoxia. HIF-1-mediated transcriptional activation and cell-specific post-transcriptional regulation. J Biol Chem. 1999;274(34):24142-24146.

57. Chepelev NL, Willmore WG. Regulation of iron pathways in response to hypoxia. Free Radic Biol Med. 2011;50(6):645-666.

58. Gao M, Monian P, Quadri N, Ramasamy R, Jiang X. Glutaminolysis and Transferrin Regulate Ferroptosis. Molecular Cell. 2015;59(2):298-308.

국문요약

H9c2 심근세포주를 이용하여 새로운 허혈-재관류 시뮬레이션 모델을 구축했다. 허혈 동안 영양분 결핍과 젖산 산증, 무산소증이 나타난다고 알려져 있다. 혈청을 사용하지 않는 전통적인 산소-글루코스 결핍 모델과는 다르게, 본 연구에서는 혈장 결핍에 따른 성장 인자와 호르몬의 결핍에 의한 효과를 방지하면서, 이 특징을 세포 배양 조건에 적용하는데 용이한 투석한 소 태아 혈청을 사용했다. 산소-글루코스 결핍 모델에서는 나타나지 않았던 재관류 시뮬레이션에 의한 괴사성 세포 사멸이 본 모델에서 나타나는 것을 확인했다. 허혈-재관류에 의한 손상은 불안정 철에 의존적인 Fenton 반응과 연관 있다는 것이 보고 되었다. 하지만 허혈 또는 재관류 동안 불안정 철이 변하는지에 대해서는 논란의 여지가 있다. 본 연구를 통해 허혈-재관류 시뮬레이션 동안 불안정 철을 관찰하고 재관류에 의한 괴사성 세포 사멸과의 연관성을 조사하였다. 허혈의 시뮬레이션을 위해 투석한 소 혈청 10% 와 함께 H9c2 세포를 저산소증과 젖산 산증에 노출시켰다. 허혈 시뮬레이션 이후, 재관류 시뮬레이션을 위해 다시 원래의 배양 배지에 노출시켰다. 괴사성 세포사멸을 확인하기 위해 Lactate dehydrogenase (LDH) 유출을 측정한 결과, LDH 유출은 허혈 시뮬레이션 동안이 아닌 재관류 시뮬레이션 초기에 급격히 증가하였다. 재관류 시뮬레이션에 의한 세포 손상과 불안정 철의 연관성을 조사하였다.

불안정 철은 Calcein-AM (형광 킬레이트제) 을 이용하여 측정하였다. 전체 불안정 철은 일반적인 상태의 세포에 거의 존재하지 않는 Fe^{3+}를 포함하여 허혈 시뮬레이션 동안 증가하였고, 함께 증가한 Fe^{2+}이 재관류 시뮬레이션 1시간 동안 Fe^{3+}으로 산화되는 것을 확인하였다. 재관류 시뮬레이션 1시간 동안 전체 불안정 철은 변화하지 않으면서 Fe^{2+}는 감소하였고 Fe^{3+}는 증가하였다. 이 결과는 Fenton reaction이 발생했을 가능성을 시사하며 이 반응은 지질 과산화 반응을 일으킬 수 있다. 지질 과산화의 여부를 확인하기 위해 BODIPY C11을 사용하였다. 그 결과, 재관류 시뮬레이션 초기에 지질 과산화가 진행되는 것을 확인하였다. 어느 철의 출처가 허혈 시뮬레이션 동안의 불안정 철의 증가에 기여하는지 조사하였다. 세포 내의 대부분 철은 철의 저장 단백질인 ferritin 철과 heme 단백질과 연관된 철로 이루어져 있기에 Ferritin의 분해 기전에 관여하는 Bafilomycin A1 (Baf A1)과 Heme의 분해 효소인 Heme oxygenase-1 (HO-1)의 억제제를 허혈 시뮬레이션 동안 사용하였다. 그 결과, Baf A1, V-ATPase 억제제가 허혈 시뮬레이션 동안의 불안정 철의 증가와 재관류 시뮬레이션에 의한 손상을 억제하였다. 이는 Autophagy에 의한 Ferritin 분해가 LIP의 증가에 영향을 미쳤을 가능성을 나타낸다. 또한, Zinc protoporphyrin (HO-1 억제제)가 불안정 철의 상승을 억제하고 재관류 시뮬레이션에 의한 손상을 감소시켰으며 이는 Heme 분해에 의한 LIP가 증가했을 가능성을 시사한다. 본 연구를 통해 기존의 산소-글루코스 결핍 모델에서 발전시킨 허혈 시뮬레이션 모델을 이용하여

허혈-시뮬레이션 동안 증가한 불안정 철이 재관류-시뮬레이션 초기 동안 Fenton 반응과 함께 지질 과산화를 일으키는 것이 재관류에 의한 세포 손상 기전임을 알아내었다.